ANOMALOUS ION TEMPERATURE AND PLASMA RESISTANCE DUE TO MHD FLUCTUATIONS IN REPUTE-1 REVERSED FIELD PINCH PLASMAS

A. FUJISAWA*, H. JI*, K. YAMAGISHI, S. SHINOHARA,
H. TOYAMA, K. MIYAMOTO
Department of Physics,
Faculty of Science,
University of Tokyo,
Tokyo, Japan

ABSTRACT. Anomalous ion temperature and plasma resistance have been studied in reversed field pinch discharges of the REPUTE-1 device. The ion temperature measured by Doppler broadening of carbon V (2271 Å) has been observed to be anomalously high in hydrogen discharges with low electron density ($\bar{n}_e \leq 0.5 \times 10^{14}$ cm^{-3}); also the plasma resistance is anomalously large in these discharges. The ion temperature and the plasma resistance are shown to increase with the MHD fluctuation level. The profiles of ion temperature and soft X-ray emission have been found to be more peaked in the lower electron density regime than in the higher one. A high ion temperature and a large plasma resistance are observed simultaneously when the profile of the soft X-ray emission I_{SX} is more peaked. If I_{SX} is mainly affected by the electron temperature profile ($I_{SX} \propto n_e^2 T_e^{3.5}$), the experimental observations are in qualitative agreement with a calculation showing that the heating power of ions is larger when the electron temperature has a more peaked profile in a magnetic configuration.

1. INTRODUCTION

In present reversed field pinch (RFP) plasmas, the energy confinement time τ_E is shorter than the thermal relaxation time between ions and electrons, τ_{ei}. A rough estimate of the ion temperature T_i attained only by the classical collisional process gives the relation $T_i \simeq (\tau_E/\tau_{ei})T_e$, which implies that the ion temperature should be lower than the electron temperature ($\tau_{ei} > \tau_E$). The observed ion temperature, however, is comparable to or even higher than the electron temperature [1–5]. In high θ discharges of ZT-40M, both the calculated neutron temperature and the O VII Doppler broadening temperature are about 1500 eV, while the electron temperature is about 300 eV [6, 7]. A direct ion heating mechanism caused by a non-collisional process should be considered to explain the high ion temperature.

The combined activity of plasma flow and magnetic field fluctuations — the 'dynamo activity' — sustains the RFP magnetic configuration against resistive decay. Ohm's law gives the following expression:

$$\vec{E} = \eta \vec{j} + \langle \delta\vec{v} \times \delta\vec{B} \rangle \qquad (1)$$

where the second term on the right hand side represents the dynamo activity, and $\langle\ \rangle$ indicates the time average on the resistive diffusion time-scale. This activity provides an energy dissipation channel without magnetic helicity loss in addition to the Ohmic dissipation channel. The experimental loop voltage has been found to be larger than that expected from Ohmic dissipation, and the loop voltage in the steady state of RFP discharges can be estimated by the magnetic helicity balance equation, including anomalous helicity dissipation in the plasma edge [8, 9].

Experiments in HBTX-1B showed that the loop voltage and the ion temperature increased when the limiter was inserted deep into the plasma [10]. A possible interpretation of this is that the insertion of the limiter increases the energy loss due to fluctuations, and this excess energy input, dissipated through fluctuations, may be transferred to the ion thermal energy by a mechanism including a large viscosity of ions [11–13] or microinstabilities [14]. However, this hypothesis is not completely confirmed by experiments, although there are a few experimental observations showing that an increase of fluctuations raises the plasma resistance [15] or causes a high ion temperature [16, 17].

Recently, Giubbilei et al. [18] suggested that extra magnetic field energy is released, which heats ions

* Present address: National Institute for Fusion Science, Furo-cho, Chikusa-ku, Nagoya, 464-01, Japan.

directly by viscous damping and which heats electrons ohmically, when a plasma with a more peaked current profile relaxes to a state with a flatter current profile. These relaxation phenomena were observed in many RFP discharges with high θ as cyclic oscillations in the sustainment phase of discharges [19–23]. Anomalously high ion temperatures are commonly observed in high θ discharges and the current profile is peaked; in this case, MHD instabilities can grow easily and high MHD activity is expected. This suggests that MHD fluctuations or a relaxation process are associated with the ion heating mechanism.

We discuss here the anomalously high ion temperature measured by Doppler broadening of carbon V and the large plasma resistance in hydrogen discharges of REPUTE-1 RFP plasmas and investigate how the observed MHD fluctuations in soft X-ray signals and in the toroidal magnetic field affect the plasma resistance and the ion temperature.

2. EXPERIMENTAL SET-UP

The REPUTE-1 device (major radius = 0.82 m, minor radius = 0.22 m) has a resistive shell with a skin time of 1 ms for vertical field penetration. The operational plasma current is usually in the range of 100–400 kA. The RFP configuration is obtained about 0.4 ms after the plasma current rise, and the plasma current reaches its maximum at about 1 ms. To obtain a longer discharge duration, the F and θ values of this experiment are chosen to be about -0.4 and 2.0, respectively, regardless of the electron density. An example of a 300 kA discharge is shown in Fig. 1.

The central chord averaged electron density $\bar{n}_e$ is measured by CO_2 laser interferometry. An array of internal poloidal magnetic probes is used to determine the poloidal mode structure of the toroidal magnetic field [24, 25]. The electron temperature T_e is measured by Thomson scattering, using a ruby laser and a soft X-ray pulse height analyser (PHA).

The radial profile of the soft X-ray emission I_{SX} can be measured with a surface barrier diode array; each detector is equipped with a 0.15 μm aluminium rectifier and has a 4 μm polypropylene filter in front of it to cut off the visible and UV part of the spectrum [19, 26]. Assuming that bremsstrahlung from a hydrogen plasma is dominant, we expect $I_{SX} \propto n_e^2 T_e^{3.5}$ for our electron temperature range, T_e = 100–200 eV [19]. The contribution of the line emission from light impurities, such as that of C V and O V, has been evaluated from a previous HBTX experiment for which

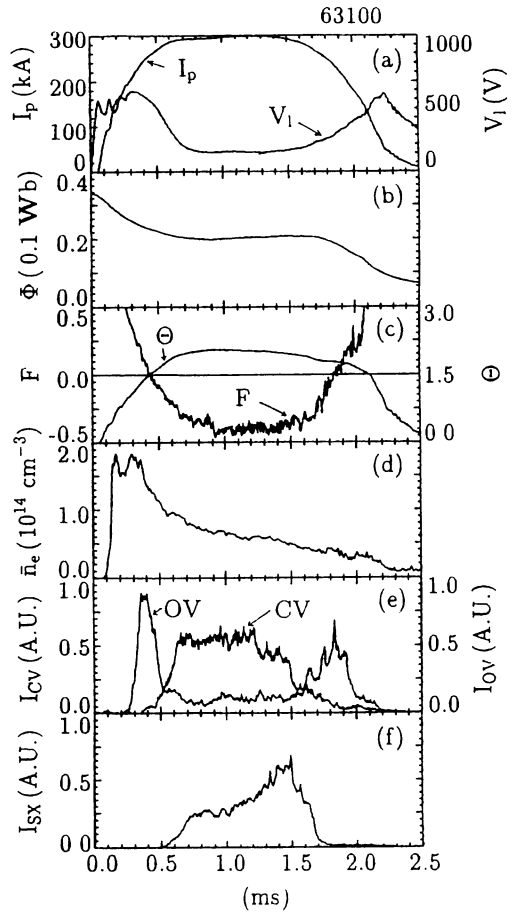

FIG. 1. Time evolution of a 300 kA RFP discharge in REPUTE-1. (a) Plasma current and loop voltage, (b) toroidal flux, (c) F and θ, (d) central chord averaged electron density, (e) C V (2271 Å) and O V (2781 Å), (f) central chord of soft X-ray emission.

$I_{SX} \propto n_e^2 T_e^{4.0}$ was reported [27]. Thus, the soft X-ray emission profile is sensitive to the electron temperature profile.

There are two eight-channel visible spectrometers which can be used to determine the ion temperature of impurities by measuring the Doppler broadening of their spectral lines. A cylindrical lens of quartz with a diameter of 2 mm, located on the exit slit, magnifies the image of the entrance slit on the surface of the detector [14]. With the cylindrical lens, the proper inverse dispersion of the two spectrometers (5.4 Å/mm) is improved to about 0.038 Å/mm.

An optical fibre light guide of 3 m, with 11 channels, is used for measuring the profiles of the C V Doppler broadening temperature. The fibres have a diameter of 200 μm and are made of quartz to transmit UV emission. The C V line is strongly attenuated ($\sim$ 15 dB/m) so that the cable length must be as short as possible,

and each channel consists of 16 optical fibre cables. The observable region of this system ranges from x = −9.0 cm to x = 9.0 cm, where x is the horizontal co-ordinate. A lens is placed in front of the light guide, and the focus of the lens is on the horizontal plane, including the plasma centre.

The C V line begins to appear when the plasma current is more than 200 kA, while the appearance of the O V (2781 Å) line is independent of the plasma current. When the plasma current is higher than 250 kA, the C V line has enough intensity to measure Doppler broadening. The plasma current in this experiment is 300 ± 10 kA, so that it is possible to determine the temperature of the C V ions. It can be seen in Fig. 1(e) that the C V line shows no sign of burn-through, while the O V line clearly exhibits burn-through already early in the discharge. Thus, we consider that the C V temperature inferred from Doppler broadening reflects the central ion temperature. Around the current flat-top, the C V (2270.9 Å) spectrum can be fitted well with a single Gaussian; however, in the termination phase of discharges, another line, presumably C II (2270.2 Å), begins to appear. Figure 2 shows a C V spectrum fitted by a single Gaussian at the current flat-top and a spectrum fitted by double Gaussians in the termination phase of discharges (t > 1.5 ms).

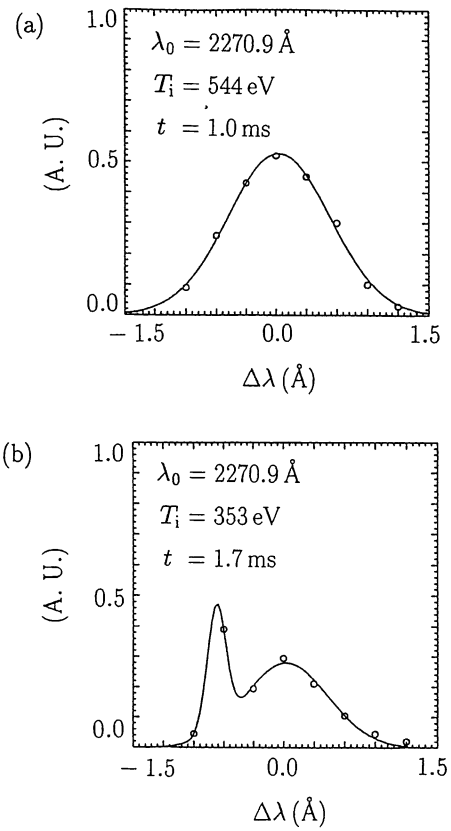

FIG. 2. Examples of C V spectra, (a) with a single Gaussian around the current flat-top, and (b) with double Gaussians in the termination phase of discharges.

3. EXPERIMENTAL RESULTS

3.1. Dependence of ion temperature and plasma resistance on the electron density

The measurements of the ion temperature T_i and the electron temperature T_e were performed 1.0 ms after the plasma current rise, which almost corresponds to the current flat-top in the case of 300 kA discharges. Figure 3 shows the dependence of T_i measured by C V (2271 Å) and T_e on the central chord averaged electron density $\bar{n}_e$. The squares are average data of the ion temperature for 50 or 60 shots (the error bars indicate the standard deviation among shots). The open and closed circles represent the electron temperatures measured by a soft X-ray PHA and by a ruby laser (Thomson scattering method), respectively. The ion temperature is strongly dependent on $\bar{n}_e$, and the relation

$$T_i\ (\mathrm{eV}) = (98.9 \pm 6.0)\bar{n}_e^{-1.4 \pm 0.1}\ (10^{14}\ \mathrm{cm}^{-3}) \qquad (2)$$

is obtained. The dependence of T_e on $\bar{n}_e$ is obviously weaker:

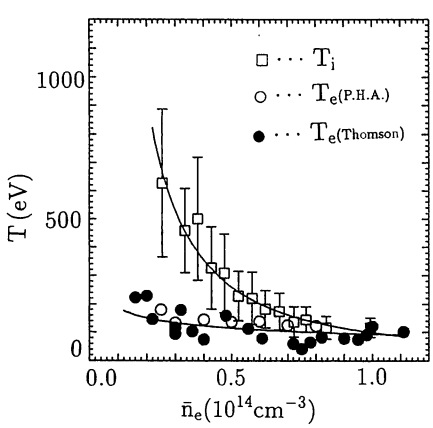

FIG. 3. Dependence of the ion temperature T_i measured by C V (2271 Å) and the electron temperature T_e on the line averaged electron density $\bar{n}_e$. The squares are data of the mean C V Doppler broadening temperature. The closed and open circles are data of the electron temperature measured by Thomson scattering and by the soft X-ray pulse height analyser, respectively. The solid lines represent $T_i(eV) = 98\ \bar{n}_e^{-1.4}$ (10^{14} cm^{-3}) and $T_e(eV) = 93\ \bar{n}_e^{-0.3}$ (10^{14} cm^{-3}).

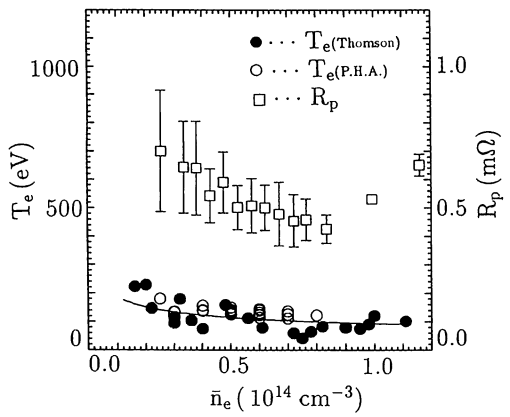

FIG. 4. Dependence of the plasma resistance R_p on the line averaged electron density $\bar{n}_e$.

$$T_e\ (\text{eV}) = (93.4 \pm 6.4)\bar{n}_e^{-0.3 \pm 0.1}\ (10^{14}\ \text{cm}^{-3}) \qquad (3)$$

The electron density in the discharges is controlled by varying the initial filling pressure, and the bank voltage is changed to adjust the current.

When $\bar{n}_e \simeq 1.0 \times 10^{14}$ cm^{-3}, both T_i and T_e are about 100 eV; the thermal relaxation time between ions and electrons is about 400 μs and the energy confinement time is about 40 μs. Since the ion temperature is expected to be about 10 eV according to the classical thermal relaxation from electrons to ions, the observed ion temperature is anomalous and it must be concluded that a direct ion heating process exists. Furthermore, the anomalous ion temperature is obviously prominent in discharges with lower electron density ($T_i/T_e \simeq 4$); for the ZT-40M experiments, T_i/T_e = 4–5 was reported [7].

Figure 4 shows the dependence of the plasma resistance R_p at t = 1.0 ms on the electron density. The plasma resistance can be calculated from the plasma current and the loop voltage V_ℓ, omitting the contribution of the plasma inductance ($R_p = (V_\ell - L_i\dot{I}_p)/I_p$, where L_i is the plasma self-inductance). The plasma resistance decreases when the electron density increases from 0.3 × 10^{14} cm^{-3} to 0.8 × 10^{14} cm^{-3} (the error bars indicate the standard deviation among shots). The electron temperature in the lower electron density regime is higher and thus, neglecting other effects such as those of the profiles of the plasma resistivity and Z_{eff}, Spitzer's formula $\eta \propto T_e^{-3/2}$ predicts that the resistance in the lower electron density regime is smaller.

Figure 5 is a plot of T_i and R_p in three different density regimes. It can be seen that the ion temperature is positively correlated with the plasma resistance; the correlation coefficient is very large (about 0.6).

3.2. MHD fluctuation versus ion temperature and plasma resistance

We examine first the dependence of T_i and R_p on fluctuations in the central chord of the soft X-ray signal. The fluctuation level of soft X-rays is defined as follows:

$$\tilde{I}_{SX} = \sqrt{\tau^{-1} \int_{t-\tau/2}^{t+\tau/2} (I_{SX} - \bar{I}_{SX})^2 dt} \qquad (4)$$

where I_{SX} and $\bar{I}_{SX}$ are the intensity of the soft X-ray and its time averaged value. This value is defined as

$$\bar{I}_{SX} = \tau^{-1} \int_{t-\tau/2}^{t+\tau/2} I_{SX} dt \qquad (5)$$

where τ = 100 μs. Figure 6 shows the dependence of T_i and R_p on the relative soft X-ray fluctuation $\tilde{I}_{SX}/\bar{I}_{SX}$. The electron density of the plotted data ranges from 0.4 × 10^{14} cm^{-3} to 0.6 × 10^{14} cm^{-3}. Each point in the figure is the average of 10–20 shots, and the error bars indicate the standard deviation among shots. The plasma resistance and the ion temperature increase with increasing soft X-ray fluctuation: the correlation coefficients range from 0.4 to 0.5. It must be noted that this correlation becomes worse in the higher electron

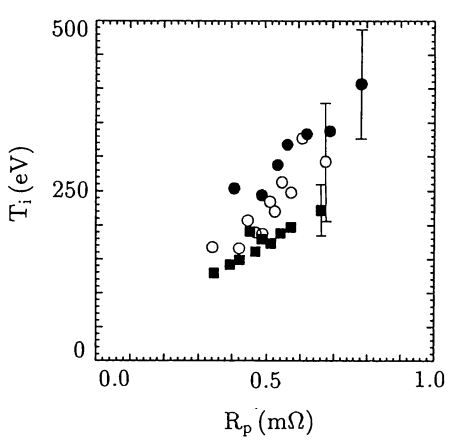

FIG. 5. Relation between the ion temperature T_i and the plasma resistance R_p. The three symbols represent the different regimes of electron density: ● — 0.4 × 10^{14} cm^{-3} ≤ $\bar{n}_e$ < 0.5 × 10^{14} cm^{-3}; ○ — 0.5 × 10^{14} cm^{-3} ≤ $\bar{n}_e$ < 0.6 × 10^{14} cm^{-3}, ■ — 0.6 × 10^{14} cm^{-3} ≤ $\bar{n}_e$ < 0.7 × 10^{14} cm^{-3}.

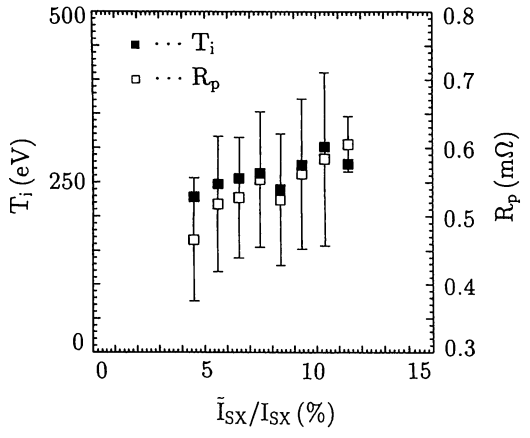

FIG. 6. Ion temperature T_i and plasma resistance R_p versus the relative fluctuation level of soft X-rays.

density regime. The fluctuation frequency ranges from about 10 kHz to 100 kHz, and mainly slower oscillations with 10–20 kHz contribute to the fluctuation amplitude. In the case of the REPUTE-1 RFP, the fluctuations with 10–20 kHz reflect sawtooth-like MHD activity caused by a competition between the resistive diffusion of the magnetic configuration and the relaxation [19, 20].

Secondly, we investigate which poloidal mode of MHD fluctuations affects the ion temperature and the plasma resistance. We use the measurement of the toroidal magnetic field with the internal magnetic probe array. The m = 1 relative amplitude is defined as

$$A_{m=1} = \frac{\Delta B_{z,m=1}}{B_{z0}} \tag{6}$$

where B_{z0} is the time averaged toroidal magnetic field and $\Delta B_{z,m=1}$ is the m = 1 component.

Figure 7 shows the dependence of T_i and R_p on $A_{m=1}$. The electron density of the plotted data ranges from 0.4×10^{14} cm^{-3} to 0.6×10^{14} cm^{-3}. Each point in the figure is the average of 10–20 shots, and the error bars indicate the standard deviation among shots. The ion temperature and the plasma resistance tend to increase with the amplitude of the m = 1 mode; the correlation coefficients range from 0.3 to 0.4. This correlation becomes worse in the higher electron density regime, as in the case of soft X-ray fluctuations. On the other hand, the ion temperature and the plasma resistance are not correlated with the relative amplitude of the m = 0 and m = 2 modes. The correlation coefficients between these modes are less than 0.1, as found by regression analysis.

3.3. Peakedness of the soft X-ray emission profile versus ion temperature and plasma resistance

The parameter which indicates the degree of peakedness of the soft X-ray emission profile is defined as the reciprocal number of the effective width σ of the profile:

$$\alpha_{SX} = \frac{a}{\sigma} \tag{7}$$

$$\sigma^2 = \sum_{i=1}^{n} (r_i - r_0)^2 f(r_i) \tag{8}$$

$$r_0 = \sum_{i=1}^{n} r_i f(r_i) \tag{9}$$

where a is the plasma radius, r_i is the radial distance of the line of sight in the i-th channel of the surface barrier detector array, and f(r) is the normalized emission profile of the soft X-ray. Note that a higher value of the peaking factor α_{SX} leads to a more peaked profile.

Figure 8a shows the dependence of α_{SX} on $\bar{n}_e$; it can be seen that the soft X-ray emission has a more peaked profile in discharges with lower electron density. The dependence of T_i and R_p on α_{SX} is shown in Fig. 8b, where the electron density of the plotted data ranges from 0.4×10^{14} cm^{-3} to 0.6×10^{14} cm^{-3}. Each point is the average of 10–20 shots, and the error bars indicate the standard deviation among shots. The ion temperature and the plasma resistance are positively correlated with the soft X-ray peaking factor; the correlation coefficient is about 0.4. A high ion temperature and a large plasma resistance are observed when the soft X-ray profile is peaked.

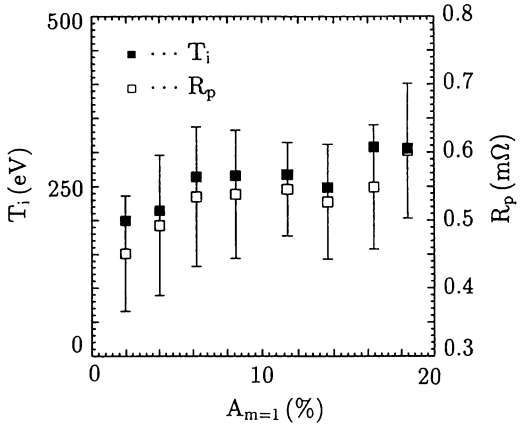

FIG. 7. Ion temperature and plasma resistance versus the relative amplitude of the poloidal m = 1 mode $A_{m=1}$, which is observed in the toroidal magnetic field.

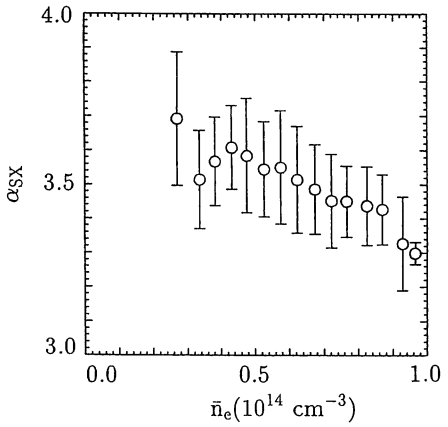

FIG. 8a. Peaking factor of the soft X-ray emission profile α_{SX} versus the electron density. The soft X-ray emission profile is found to be more peaked in the lower electron density regime.

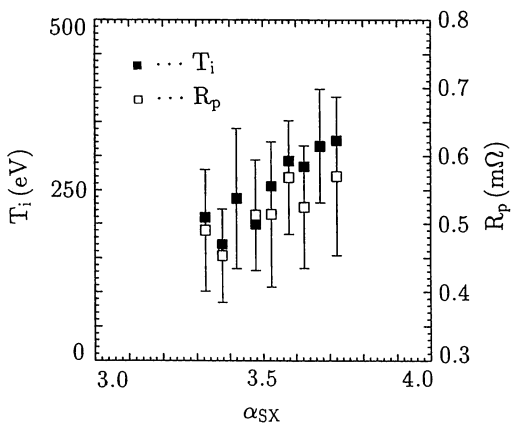

FIG. 8b. Ion temperature and plasma resistance versus the peaking factor of the soft X-ray profile.

The results of the measurement of the ion temperature profiles from C V (2271 Å) have been obtained with the light-guide system of optical fibres. Figure 9 shows the ion temperature profiles without Abel inversion, in three different regimes of the electron density. The solid lines are the fitting curves, for which

$$T_i(r) = T_i(0)(1 - (r/a)^p)^q \qquad (10)$$

where $T_i(0)$, p and q are fitting parameters. In case (a) of Fig. 9, T_i = 270 eV, p = 2, q = 3; in case (b), $T_i(0)$ = 230 eV, p = 4, q = 14. In case (c), the ion temperature in the observable range is constantly 170 eV, and the ion temperature profile cannot be fitted by this function. Figure 10 shows the Doppler broadening temperatures of other carbon ions with lower ionization potential — C III (4647 Å) and C IV (4658 Å). The temperatures are less than 100 eV and are almost independent of the electron density. Thus, we conclude that the ion temperature profile becomes more peaked in the low electron density regime.

4. DISCUSSION

4.1. Anomalous ion temperature and plasma resistance in the low electron density regime

Similar to other RFP experiments [14], our experimental results show that the C V Doppler broadening temperature has a strong dependence on $\bar{n}_e$ ($T_i \propto n_e^{-1.4}$). The electron temperature, however, has a weak dependence on $\bar{n}_e$ ($T_e \propto n_e^{-0.4}$), while other RFP experiments showed that the electron temperature has a strong dependence on the electron density. It is possible

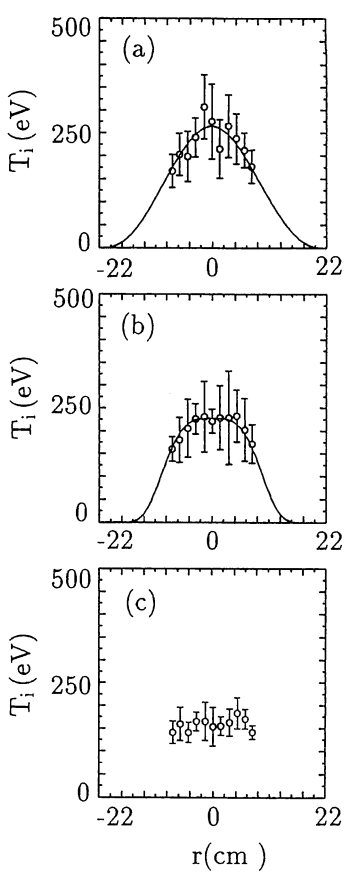

FIG. 9. Ion temperature profiles without Abel inversion measured from the C V (2271 Å) line.
(a) 0.4 × 10^{14} cm^{-3} ≤ $\bar{n}_e$ < 0.5 × 10^{14} cm^{-3}
(b) 0.5 × 10^{14} cm^{-3} ≤ $\bar{n}_e$ < 0.6 × 10^{14} cm^{-3}
(c) 0.6 × 10^{14} cm^{-3} ≤ $\bar{n}_e$ < 0.7 × 10^{14} cm^{-3}.

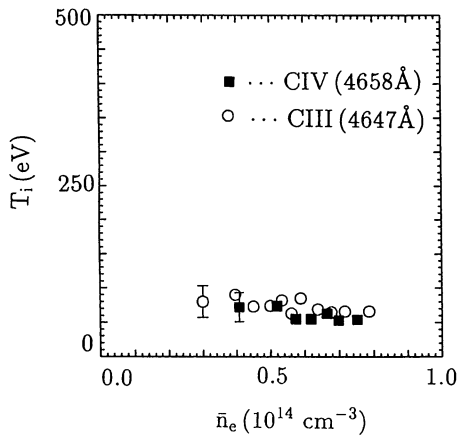

FIG. 10. Doppler broadening temperatures of carbon ions with lower ionization potential.

that in low electron density discharges the C V Doppler broadening temperature is different from the hydrogen temperature, which is the main ion temperature of our plasma. The thermal relaxation time between H^+ and C^{4+} is

$$\tau_{rel}^{C^{4+}-H^+}\ [\mu s] = \frac{8.1 \times 10^{-3}}{n_H}\left(T_i^H + \frac{T_i^{CV}}{12}\right)^{3/2}$$

where n_H is the hydrogen density in 10^{14} cm^{-3}. When $n_H \simeq 0.1 \times 10^{14}$ cm^{-3}, $T_i^H \simeq 100$ eV and $T_i^{CV}/12 < T_i^H$, the relaxation time is about 80 μs. Since the energy confinement time of REPUTE-1 RFP plasma is less than 100 μs in the low electron density regime, the C V Doppler broadening temperature does possibly not relax to the hydrogen temperature if the heating power rates of different species are not the same.

The anomalously large resistance is strongly correlated with the anomalous ion temperature, and the plasma resistance is given by

$$R_p\ (\Omega) = \eta_0\left(\frac{2\pi R}{\pi a^2}\right)\xi_k + R_p^{edge}$$

$$= 5.23 \times 10^{-5}\frac{Z_{eff}\ln\Lambda}{T_e[eV]^{3/2}}\left(\frac{2\pi R}{\pi a^2}\right)\xi_k + R_p^{edge} \quad (11)$$

where ln Λ is the Coulomb logarithm, ξ_k is a profile factor calculated by the helicity balance equation without anomalous helicity dissipation, and R_p^{edge} is the plasma resistance due to anomalous helicity dissipation in the plasma edge. When the empirical scaling law of T_e with $\bar{n}_e$ (Eq. (3)) is inserted into Eq. (11), the dependence of R_p on $\bar{n}_e$ is given by

$$R_p\ (m\Omega) = 0.26 \times 10^{-1}\ Z_{eff}\ \xi_k\ \bar{n}_e^{0.45} + R_p^{edge} \quad (12)$$

where n_e is in 10^{14} cm^{-3}. In the ZT-40M experiments, the relation between plasma resistivity and electron density $\eta \propto \bar{n}_e^{0.7}$ was found [28].

Equation (12) shows that the large plasma resistance in the lower electron density regime may be caused by a change of the electron temperature profile (corresponding to ξ_k), an increase in Z_{eff} and an increase in the anomalous helicity dissipation in the plasma edge (corresponding to R_p^{edge}). The effect of a change of the current profile on ξ_k is neglected, since the F and θ values in this experiment are fixed at -0.4 and 2.0, respectively. We have already shown the significant positive correlation of T_i and R_p with α_{SX}. Since the emission profile of soft X-rays is sensitive to the electron temperature, as noted previously, we consider that the large α_{SX} is caused by the peaked profile of the electron temperature. We have calculated the effect of the electron temperature profile on the profile factors ξ_k and ξ_w, which are related to the total plasma resistance and to the plasma resistance including only Ohmic dissipation, respectively (see Appendix).

In the calculation, the electron temperature profile is assumed to be

$$T_e(r) = (T_e(0) - T_e(a))\ (1 - (r/a)^2)^\beta + T_e(a)$$

$$T_e(a) = 0.1\ T_e(0) \quad (13)$$

where the parameter β determines the peakedness of the electron temperature profile. The magnetic configuration is determined by a modified Bessel function model, with the assumption that the pressure is zero and $\mu(r) = 2\theta_0/a(1 - (r/a)^2)^\alpha$, and the anomalous helicity dissipation in the plasma edge is neglected. Figure 11 shows the profile factors ξ_k, ξ_w, $\Delta\xi(=\xi_k - \xi_w)$ as a function of β. It is assumed that $\alpha = 1.25$ and $\theta_0 = 2.14$ (corresponding to F = -0.4 and $\theta = 2.0$), which are typical values of REPUTE-1 discharges. Both profile factors increase with β. This calculation shows that the profile factor ξ_k is larger when the plasma has a more peaked electron temperature profile (larger β). Thus, the larger plasma resistance in the lower electron density regime can be ascribed to the increase in ξ_k due to the more peaked profile of the electron temperature. Moreover, the rate of $\Delta\xi$ increasing with β is larger than that of ξ_w, i.e. the heating power of ions increases more rapidly than that of electrons with an increase in the peakedness of the electron temperature profile, on the basis of the

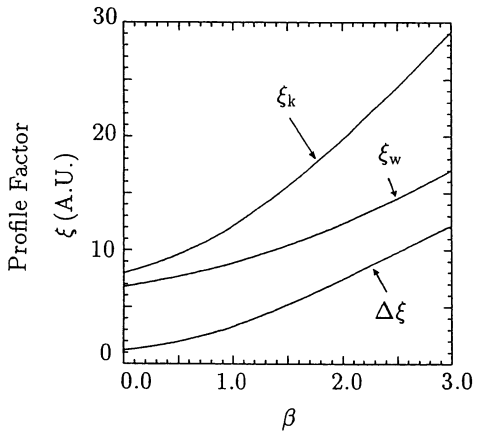

FIG. 11. Calculation results for the profile factors ξ_k, ξ_w and $\Delta\xi$ as a function of the electron temperature profile determined by the parameter β (see Eq. (13)).

assumption that the energy dissipation due to fluctuations and the Ohmic dissipation contribute to ion and electron heating, respectively. This is consistent with the experimental result that direct ion heating becomes more prominent in the lower electron density regime if the energy confinement time of ions is not much changed.

Assuming that the local heating powers of ions and electrons are represented by $-\langle\delta\vec{v} \times \delta\vec{B}\rangle \cdot \vec{j}$ and $\eta\vec{j}^2$, respectively, the heating power profiles of ions and electrons can also be calculated as a function of β. The heating power profiles are shown in Fig. 12. When the electron temperature profile becomes more peaked (larger β), the heating power profile of ions is more peaked, so that the ion temperature profile should also become peaked if the ion energy diffusion profile is not drastically changed. Although the contribution of Z_{eff} and R_p^{edge} can be neglected, these calculation results are qualitatively consistent with our experimental results that the ion temperature has a more peaked profile and an anomalously high value in the lower electron density regime.

4.2. Ion heating due to MHD fluctuations

The soft X-ray fluctuations observed in this experiment indicate the intensity of the sawtooth-like oscillations caused by the relaxation process. The significant positive correlation between the ion temperature and the soft X-ray fluctuation level supports the assumption that the energy released during the relaxation process is directly used for ion heating. Experimental and simulation studies show that in the relaxation process the m = 1 instability is the driving force of the magnetic field reconnection; many studies proposed that a non-linear reconnection process is essential for the relaxation phenomena of RFP plasmas [29–33]. We have found that the large amplitude of the m = 1 mode is associated with the high ion temperature and the large plasma resistance. This indicates that the kinetic energy of plasma flow driven by the m = 1 instability is transferred to the ion thermal energy during the relaxation process.

Assuming that the velocity of plasma flow u is 0.03 times as large as the Alfvén velocity in our 300 kA discharges and that this kinetic energy is transferred to the ion thermal energy in the relaxation time τ_{rel}, the heating power density of ions is

$$Q_i = \frac{1/2\rho_m u^2}{\tau_{rel}} = 18\ \mathrm{MW/m^3} \qquad (14)$$

where ρ_m is the mass density; the plasma parameters used are given in Table I. The assumed plasma flow velocity is acceptable, since a growth rate calculation of the m = 1 internal kink modes has confirmed that

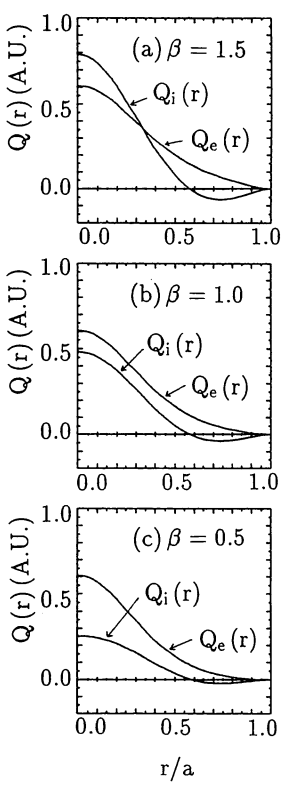

FIG. 12. Heating power profiles of ions and electrons, $Q_i(r)$ and $Q_e(r)$ in three different cases of electron temperature profile determined by the parameter β (see Eq. (13)). (a) β = 1.5, (b) β = 1.0, (c) β = 0.5.

TABLE I. PLASMA PARAMETERS OF 300 kA RFP discharges in REPUTE-1

Plasma current, I_p	300 kA
Loop voltage, V_ℓ	150 V
Plasma volume, V_p	0.78 m^3
Input power density, I_pV_ℓ/V_p	58 MW/m^3
Central magnetic field, B_0	0.5 T
Plasma density, n_e	7.5×10^{19} m^{-3}
Alfvén velocity, v_A	1.5×10^6 m/s
Relaxation time, τ_{rel}	20 μs

the velocity of the plasma flow driven by the instabilities can reach values that are 0.1 times as large as the Alfvén velocity [34]. The total heating power of plasma can be estimated from the plasma current and the loop voltage as

$$Q_{total} = \frac{I_pV_\ell}{V_p} = 58 \text{ MW/m}^3 \quad (15)$$

where V_p is the plasma volume. The ratio of Q_i to Q_{total} is about 0.3. Figure 11 shows that the ratio of $\Delta\xi$ to ξ_k is about 0.3 when $\beta = 2.0$. The kinetic energy of the plasma flow is sufficient to be a source for the ion thermal energy.

The question is how the kinetic energy of the plasma flow is transferred to the ion thermal energy. One of the most likely possibilities is viscous damping; the ion viscosity is about m_i/m_e ($\simeq 1800$ in the case of hydrogen) times larger than the electron viscosity; the ions are heated preferentially by viscous damping. It cannot be excluded, however, that other possible mechanisms, such as microinstabilities and stochastic heating, participate in the direct ion heating. In a cascade process, the energy of the fluctuating electric field (together with the fluctuating magnetic field) with a small wave number is continuously transferred to the field with a large wave number, and the energy of the stochastic electric field with a large wave number is absorbed at the ion cyclotron frequency [35].

Our experiments have led us to the conclusion that the MHD fluctuations associated with the relaxation phenomena, or the dynamo activity, are probably responsible for the anomalous ion temperature and the anomalous plasma resistance, and that the energy released during the relaxation process is transferred to the ion thermal energy.

5. CONCLUSIONS

The ion temperature measured by C V (2271 Å) Doppler broadening has been found to be anomalously high compared with the electron temperature measured by Thomson scattering and a soft X-ray PHA in the lower electron density regime ($\bar{n}_e < 0.5 \times 10^{14}$ cm^{-3}). The high ion temperature is correlated with a large plasma resistance caused by an increase in the MHD fluctuation level. The ion temperature and the soft X-ray emission (which is considered to reflect the electron temperature profile) have more peaked profiles in the lower electron density regime. The calculations have shown that the ion heating power should increase and its profile should become more peaked as the electron temperature profile becomes more peaked. These results show that the energy dissipated by the MHD fluctuations is transferred to the ion thermal energy, and the m = 1 mode is suggested to play an important role in the direct ion heating mechanism.

Appendix

PLASMA RESISTANCE OF RFP PLASMAS

The plasma resistance of RFP plasmas is divided into two components (see Refs [8, 9]): Ohm's law for RFPs is given as

$$\eta\vec{j}_0 = \vec{E}_0 + \langle\delta\vec{v} \times \delta\vec{B}\rangle \quad (A.1)$$

in the sustainment phase. Executing the integral of Eq. (A.1) multiplied by $\vec{j}$, we obtain the energy balance equation:

$$V_\ell I_p = \int \eta\vec{j}^2\,dv + \int -\langle\delta\vec{v} \times \delta\vec{B}\rangle\cdot\vec{j}dv \quad (A.2)$$

where $V_\ell = 2\pi RE_z$ is the loop voltage and I_p is the toroidal plasma current and z represents the toroidal direction. In terms of the plasma resistance, Eq. (A.2) can be rewritten as

$$R_pI_p^2 = R_{pe}I_p^2 + \Delta R_pI_p^2 \quad (A.3)$$

$$R_{pe}I_p^2 = \eta_0\left(\frac{2\pi R}{\pi a^2}\right)\xi_wI_p^2 = \int \eta\vec{j}^2dv \quad (A.4)$$

$$\Delta R_pI_p^2 = \eta_0\left(\frac{2\pi R}{\pi a^2}\right)\xi_kI_p^2 + R_p^{edge}I_p^2 = \int -\langle\delta\vec{v} \times \delta\vec{B}\rangle\cdot\vec{j}dv \quad (A.5)$$

The first and the second terms on the right hand side of Eq. (A.3) represent the plasma resistance due to the Ohmic dissipation and that due to the fluctuations, respectively. In Eqs (A.4) and (A.5), ξ_k is the profile factor for helicity dissipation, ξ_w is the profile factor for Ohmic dissipation, η_0 is the plasma resistivity at the centre and R_p^{edge} is the plasma resistance due to anomalous helicity dissipation in the plasma edge. The total plasma resistance can be calculated by the magnetic helicity balance equation:

$$V_\ell \Phi_z = \int \eta \vec{j} \cdot \vec{B} dv - \frac{1}{2} \int \phi \vec{B} \cdot \vec{dS} \qquad (A.6)$$

where Φ_z is the toroidal flux and ϕ is the scalar potential of the electric field.

On the basis of the hypothesis that the Ohmic dissipation and the dissipation by the fluctuations contribute to the heating of electrons and ions, respectively, the local heating powers of electrons $Q_e(r)$ and ions $Q_i(r)$ can be defined as

$$Q_e(r) = \eta(r) \vec{j}(r)^2 \qquad (A.7)$$

$$Q_i(r) = -\langle \delta \vec{v} \times \delta \vec{B} \rangle \cdot \vec{j} = \vec{E} \cdot \vec{j}(r) - \eta(r) \vec{j}(r)^2 \qquad (A.8)$$

where $\eta(r)$ is the radial profile of the plasma resistivity.

ACKNOWLEDGEMENTS

The authors are grateful to Dr. Y. Nagayama for his advice and discussions of spectroscopic systems. Also, they would like to thank Y. Shimazu, A. Ejiri, A. Shirai, S. Ohdachi and K. Mayanagi for their help in the experiments.

REFERENCES

[1] CAROLAN, P.G., ALPER, B., BEVIR, M.K., et al., in Plasma Physics and Controlled Nuclear Fusion Research 1984 (Proc. 10th Int. Conf. London, 1984), Vol. 2, IAEA, Vienna (1985) 449.

[2] TAMANO, T., BARD, W.D., CARLSTROM, T.N., et al., ibid., p. 431.

[3] HIRANO, Y., KONDOH, Y., MAEJIMA, Y., et al., ibid., p. 475.

[4] ALPER, B., TSUI, H.Y.W., in Controlled Fusion and Plasma Physics (Proc. 14th Eur. Conf. Madrid, 1987), Vol. 11D, Part II, European Physical Society (1987) 434.

[5] FUJISAWA, A., NAGAYAMA, Y., YAMAGISHI, K., et al., in Controlled Fusion and Plasma Heating (Proc. 15th Eur. Conf. Dubrovnik, 1988), Vol. 12B, Part II, European Physical Society (1988) 549.

[6] WURDEN, G.A., WEBER, P.G., SCHOENBERG, K.F., et al., ibid., p. 533.

[7] WURDEN, G.A., SCHOENBERG, K.F., PICKRELL, M.M., et al., in Physics of Mirrors, Reversed Field Pinches and Compact Tori (Proc. Course and Workshop Varenna, 1987), Vol. 1, Editrice Compositori, Bologna (1988) 159.

[8] SCHOENBERG, K.F., MOSES, R.W., Phys. Fluids **27** (1984) 1671.

[9] TSUI, H.Y.W., Nucl. Fusion **28** (1988) 1543.

[10] CAROLAN, P.G., FIELD, A.R., LAZAROS, A., et al., in Controlled Fusion and Plasma Physics (Proc. 14th Eur. Conf. Madrid, 1987), Vol. 11D, Part II, European Physical Society (1987) 469.

[11] MIYAMOTO, K., Plasma Phys. Control. Fusion **30** (1988) 1493.

[12] LAZAROS, A., Plasma Phys. Control. Fusion **31** (1989) 1995.

[13] GIMBLETT, C.G., Europhys. Lett. **11** (1990) 541.

[14] HOWELL, R.B., NAGAYAMA, Y., Phys. Fluids **28** (1985) 743.

[15] ALPER, B., MARTIN, P., in Controlled Fusion and Plasma Physics (Proc. 16th Eur. Conf. Venice, 1989), Vol. 13B, Part II, European Physical Society (1989) 725.

[16] SHIMADA, T., YAGI, Y., HIRANO, Y., et al., in Plasma Physics and Controlled Nuclear Fusion Research 1988 (Proc. 12th Int. Conf. Nice, 1988), Vol. 2, IAEA, Vienna (1989) 457

[17] SCHOENBERG, K.F., INGRAHAM, J.C., MOSES, R.W., Jr., et al., ibid., p. 419.

[18] GIUBBILEI, M., MARTIN, P., ORTOLANI, S., Plasma Phys. Control. Fusion **32** (1990) 405.

[19] ASAKURA, N., NAGAYAMA, Y., SHINOHARA, S., et al., Nucl. Fusion **29** (1989) 893.

[20] UEDA, Y., ASAKURA, N., MATSUZUKA, S., et al., Nucl. Fusion **27** (1987) 1453.

[21] ANTONI, V., ORTOLANI, S., Phys. Fluids **30** (1987) 1489.

[22] ANTONI, V., MARTIN, P., ORTOLANI, S., Nucl. Fusion **29** (1989) 1759.

[23] WATT, R.G., NEBEL, R.A., Phys. Fluids **26** (1983) 1168.

[24] JI, H., TOYAMA, H., SHINOHARA, S., et al., in Controlled Fusion and Plasma Physics (Proc. 16th Eur. Conf. Venice, 1989), Vol. 13B, Part II, European Physical Society (1989) 733.

[25] JI, H., TOYAMA, H., SHINOHARA, S., et al., Plasma Phys. Control. Fusion **32** (1990) 79.

[26] SHIMAZU, Y., SHINOHARA, S., FUJISAWA, A., et al., in Controlled Fusion and Plasma Heating (Proc. 17th Eur. Conf. Amsterdam, 1990), Vol. 14B, Part II, European Physical Society (1990) 549.

[27] MALACARNE, M., HUTCHINSON, I.H., Plasma Phys. Control. Fusion **29** (1987) 823.

[28] WURDEN, G.A., WEBER, P.G., WATT, R.G., et al., in Physics of Mirrors, Reversed Field Pinches and Compact Tori (Proc. Course and Workshop Varenna, 1987), Vol. 1, Editrice Compositori, Bologna (1988) 411.

[29] COLGATE, S.A., FERGUSON, J.F., FURTH, H.P., in Peaceful Uses of Atomic Energy (Proc. 2nd Int. Conf. Geneva, 1958), Vol. 32, UN, New York (1958) 129.
[30] SYKES, A., WESSON, J., in Controlled Fusion and Plasma Physics (Proc. 8th Eur. Conf. Prague, 1977), Vol. 1, Part I, Institute of Plasma Physics, Czechoslovak Academy of Sciences, Prague (1977) 80.
[31] CARAMANA, E.J., NEBEL, R.A., SCHNACK, D.D., Phys. Fluids **26** (1983) 1305.
[32] SATO, T., KUSANO, K., Phys. Rev. Lett. **54** (1985) 808.
[33] KUSANO, K., SATO, T., Nucl. Fusion **26** (1986) 1051.
[34] FUJISAWA, A., ONODERA, S., MIYAMOTO, K., J. Phys. Soc. Jpn. **58** (1989) 473.
[35] PURI, S., Phys. Fluids **9** (1966) 2043.

(Manuscript received 22 October 1990
Final manuscript received 7 March 1991)